metals

MDPI

Article

Heat Input Influence on the Fatigue Life of Welds from Steel S460MC

Jaromir Moravec *, Jiri Sobotka, Pavel Solfronk and Robin Thakral

Faculty of Mechanical Engineering, Department of Engineering Technology, Technical University of Liberec, Studentská 1402/2, 46117 Liberec, Czech Republic; jiri.sobotka@tul.cz (J.S.); pavel.solfronk@tul.cz (P.S.); robin.thakral@tul.cz (R.T.)

* Correspondence: jaromir.moravec@tul.cz; Tel.: +420-485-353-341

Received: 13 September 2020; Accepted: 24 September 2020; Published: 25 September 2020

Abstract: Fine-grained steels belong to the progressive materials, which are increasingly used in the production of welded structures subjected to both static and dynamic loads. These are unalloyed or microalloyed steels hardened mainly by the grain-boundary strengthening mechanism. Such steels require specific welding procedures, especially in terms of the heat input value. At present, there are studies of the welding influence on the change of thermomechanically processed steels' mechanical properties, however mainly under static loading. The paper is therefore focused on the assessment of the welding effect under dynamic loading of welded joints. In the experimental part was determined the influence of five different heat input values on the change of weld fatigue life. As a result, there is both determination of five S-N curves for the double-sided fillet welds from the thermomechanically processed fine-grained steel S460MC and the quantification of the main influences reducing the fatigue life of the joint.

Keywords: heat input; welding; fatigue life; fine-grained steel S460MC; S-N curves

1. Introduction

In today's modern and innovative times, more and more demands are placed on industrially used materials. In addition to that, materials are often required to fulfil conflicting properties, such as, e.g., to have high yield strength, ultimate tensile strength, and simultaneously also good ductility, formability, or weldability. At the same time, high attention is paid as well to the price of these materials, which increases with the amount of used alloying elements. Therefore, newly developed materials use a grain-boundary strengthening and belong to the group of so-called HSLA (High Strength Low Alloy) steels. These are usually microalloyed fine-grained steels that are alloyed by very low contents of elements such as, e.g., V, Ti, and Nb. Such elements form fine carbides, nitrides, or carbonitrides and contribute to the grain refinement and strengthening of the matrix [1,2]. It also has a secondary effect in increased values of the yield strength and ultimate tensile strength, but there is also lower values of transient temperature and brittle fracture properties [3,4]. Moreover, despite all of the advantages mentioned above, these steels also keep their price low, because they are derived from the prices of conventional carbon steels due to the low amount of alloying elements.

Although many people think of HSLA steels primarily as high-strength steels, typically with yield strengths highly exceeding 550 MPa, micro-alloyed steels are very popular and often used in the production of structures having yield strength below 550 MPa. Among these can be found, for example, thermomechanically processed steels of the S355MC, S420MC, and S460MC types. As a reason why these steels gradually substitute the common structural steels (e.g., type S355J2), there is their better cold formability and constant technological processability given by stronger demands to meet their chemical composition.

Generally, HSLA steels reveal good weldability, but the amount of heat input into the weld should be limited and should not exceed 15 kJ·cm^{-1}. In the case of high-strength steels, it is recommended to further reduce such heat input value. As a reason for that, there is the intensive grain coarsening in the heat-affected zone (HAZ) at temperatures over 1100 °C. These are temperatures at which occurs dissolving of the fine precipitates that stabilize grain boundaries and structure. Such an issue is quite a closely monitored topic that confirms also a great number of published articles dealing with the grain coarsening intensity [2,4,5], changes in strength and brittle-fracture properties [4,6,7], or structural changes that occur in the heat-affected zone—HAZ [8,9]. However, not many papers are devoted to the influence of welding on changes in the fatigue life of welded joints for HSLA steels with a yield strength lower than 550 MPa [10], despite the fact that these materials and welded structures are used very often—for example, in land transportation [11] (i.e., in areas of quite intense dynamic loading). Nevertheless, more works are devoted to welded joints of high-strength materials [12–14] and again despite the fact that the notch effect arising from the weld geometry reduces its fatigue life to the level of welded joints with lower values of yield strength.

Most works dealing with the fatigue tests of HSLA steel welded joints [12,15] use for fatigue tests either butt welds or flat specimens to which a temperature cycle is applied. This is a little bit strange, because most dynamically loaded structural units used in the field of land transportation contain mainly fillet welds, despite their lower static and dynamic load capacity. Other works then deal, e.g., with the influence of load cycle asymmetry—stress ratio R [16] or fatigue life prediction using the energy approach [13].

The aim of the research described in the following sections, was to point out that there have not been almost any papers published dealing with the welded joints from steel S460MC. Thus, the aim was to assess the heat input influence on the fatigue life of fillet welded joints that are structurally designed to match the joints commonly used in industrial production. As a result, complete S-N curves were obtained at stress amplitudes corresponding to the range of loading cycles from 10^4 up to 10^7. Most authors studying the HSLA steel welds' fatigue life usually focus on the butt welds from the high-strength steels. If they deal with the fillet welds, there are performed fatigue tests at selected stress amplitudes within the loading cycles from 10^5 up to 2×10^6 [17], and for the remaining stress amplitudes are just used an approximation of the fatigue curves or there are used cruciform welds at testing [18,19]. These welds are due to their symmetry of four fillet welds more suitable in light of our own testing. However, they are completely unsuitable from the welding point of view, especially for the fine-grained steels. In addition to that, very important is also knowledge about mutual proportion among the yield strength, fatigue limit of the base material $\sigma_{c(BM)}$, and fatigue limit of the fillet welded joint $\sigma_{c(W)}$ from steel S460MC and its comparison with the (ultra) high-strength steels, presented by other authors.

2. Tested Material and Experimental Methods

The major aim of the experimental part was to determine the influence of heat input from welding on the fatigue life of welded joints. In the case of arc welding methods, heat input value is given by the process parameters (welding current, voltage, welding speed, etc.) and therefore has a strong influence on the weld pool geometry as well as on the size and structure of HAZ. Changes that occur in HAZ of welds have a significant effect on the mechanical properties of our own welded joint, as well as on the magnitude of the Charpy impact energy KV_2 [4,6,9].

Nevertheless, studies on how these changes are affecting the fatigue life of S460MC fine-grained steel fillet joints have not been published anywhere. In addition to that, this steel is very often used for structures subjected to both static and dynamic loading. As examples there can be mentioned truss structures of bridges, building cranes, axle parts of cars and trucks, or, e.g., various components of rail vehicles.

Used steel S460MC is a fine-grained, thermomechanically processed structural steel with a ferritic-pearlitic structure, as shown in Figure 1. It has a low content of carbon and elements such as S and P, and exhibits good weldability. Chemical composition of the tested steel S460MC determined

by the spectrometer Q4 TASMAN (Bruker, Germany) is shown in Table 1. Measured chemical composition is in accordance with the standard EN 10149-2 indicating chemical composition of the thermomechanically processed structural steels.

Table 1. Chemical composition of the tested material—steel S460MC.

Chemical Element	C	Mn	Si	P	S	Nb	W	Ni	V	Cr	Ti
Composition [wt %]	0.07	1.32	0.01	0.03	0.01	0.05	0.04	0.04	0.08	0.01	0.01

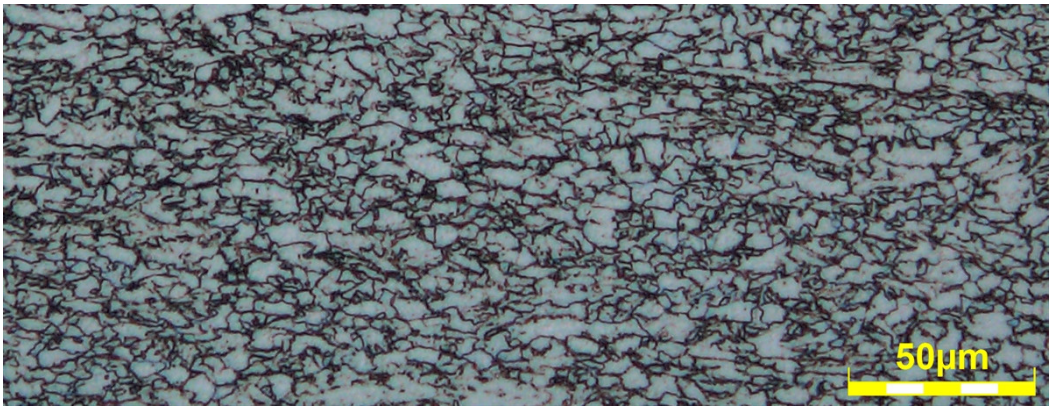

Figure 1. Metallographic structure of the base material—steel S460MC.

Subsequently, the mean grain size of 7.3 µm was determined from the EBSD analysis. This is the average value obtained from three measurements of areas 0.6 mm × 0.6 mm. Table 2 shows the basic mechanical properties measured by the static tensile test and in this case are results taken as the average of five measurements.

Table 2. Basic mechanical properties of tested material—steel S460MC.

Mechanical Properties	Yield Strength R_e [MPa]	Ultimate Tensile Strength R_m [MPa]	Uniform Ductility A_g [%]	Total Ductility A_{30} [%]
EN 10149-2	Min. 460	520–670	X	Min. 17
Measured values	544 ± 17	629 ± 21	13.15 ± 0.42	29.03 ± 0.91

To assess the fatigue properties of the tested material, there was determined the S-N curve of the base material. All fatigue tests of the base material were performed on the servo-hydraulic testing machine INOVA FU-O-1600-V2 (having maximum achievable force load as 100 kN, INOVA GmbH, Bad Schwalbach, Germany) in the controlled force mode. For all experiments, there were used samples having a circular cross-section in accordance with standard EN 3987—see Figure 2.

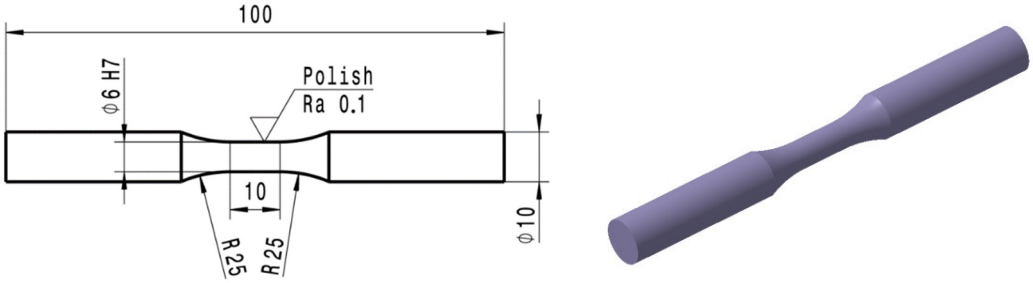

(**a**) (**b**)

Figure 2. Dimensions and (**b**) 3D illustration of testing sample according to standard EN 3987. (unit: mm).

Testing samples were subjected to the selected stress amplitudes under a fully reversed harmonic cycle (purely alternating stress) with the stress ratio R = −1 (algebraic ratio of the minimum stress to the maximum stress) and frequency 40 Hz. Testing frequency was chosen on the basis of previously performed tests with the same type and geometry of testing sample. As a criterion, there was taken a sufficiently high frequency at which the sample surface had not been heated up to yet. To properly adjust such frequency, the sample surface was scanned by the infrared pyrometer Mikro-epsilon CTLM-3H2CF2-C8H (Micro-Epsilon Messtechnik, Germany), having the temperature range from −60 up to 200 °C. This surface (with a shape and dimensions corresponding to Figure 2) was heated up at frequency of 55 Hz. Own testing was performed at stress amplitudes 450 and 350 MPa. The magnitude of the stress amplitudes was constant for every used stress level. As a criterion for terminating the test, there was taken initialization of the fatigue crack or achieving so-called fatigue (endurance) limit at 10^7 cycles, where the material can endure an infinite number of cycles without failure. A total of 21 samples were tested under the following stress amplitudes (levels): 450, 400, 375, 350, 343, 337.5, 325 and 312.5 MPa. Based upon these results, there was subsequently determined the fatigue limit of base material as $\sigma_{c(BM)}$ = 340 MPa. The final S-N curve of the base material is shown in Figure 3.

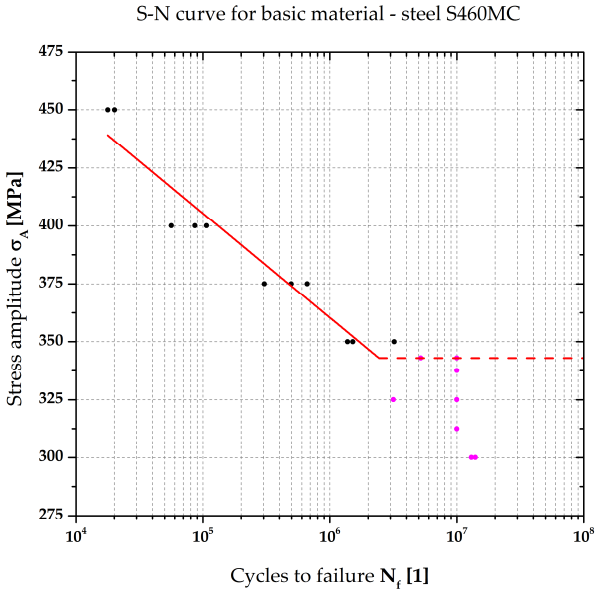

Figure 3. S-N curve (semi-log scale) of the base material—steel S460MC.

3. Welding of Testing Samples

For our own experimental testing, double-sided fillet welds were firstly designed and then assembled from semi-finished products having the following dimensions: 300 mm × 190 mm × 10 mm in the case of flange and 300 mm × 110 mm × 10 mm for the web. The web was milled in the contact areas with the flange so that the contact between them was even along its entire length. After that, there was used semi-automatic MAG welding method in the PA position, while the angle between torch and flange was 30°. As a filler material, there was used an OK Autrod 12.51 with a diameter of 1.2 mm and shielding gas M21 according to ISO 14175 with a flow rate 15 L·min^{-1}. The welding parameters were adjusted on the basis of the previous experiments so that the heat input values for the individual welds reached the following magnitudes: 8, 9, 10, 12 and 14 kJ·cm^{-1}. Heat input into the weld in the arc welding method is given as the product of voltage and current, divided by the welding speed. In the case of welding, unit kJ·cm^{-1} is most often used for the heat input value. For welding was also used the power supply Migatronic BDH 550 Puls Sync in the synergic mode with a distance between contact die and welding point as 14 mm. In Table 3, the major adjusted welding parameters are shown, which were always the same for both weld beads on the relevant weld. For

better readability, notation of the individual samples was derived according to the heat input values (Q = 8, 9, 10, 12, and 14 kJ·cm^{-1})—thus as Weld Q8, Q9, Q10, Q12 and Q14.

Table 3. Process parameters adjusted on the power supply and linear automat.

Weld Designation	Current I [A]	Welding Speed v_s [m·min^{-1}]	Expected Voltage U [V]	Calculated Heat Input Q [J·cm^{-1}]
Weld Q8	260	0.505	26.0	8.03
Weld Q9	320	0.600	28.1	8.99
Weld Q10	260	0.400	25.7	10.02
Weld Q12	250	0.300	23.9	11.95
Weld Q14	265	0.295	26.0	14.01

Welding parameters were monitored by the system WeldMonitor (DIGITAL ELECTRIC, Brno, Czech Republic) at scanning frequency 20 kHz. Table 4 shows the measured effective values of voltage, current, and welding speed for all weld beads.

Table 4. Actual process parameters measured by the system WeldMonitor.

Weld Designation	Number of Bead	Effective Current I [A]	Effective Voltage U [V]	Real Welding Speed v_s [m·min^{-1}]	Heat Input Q [J·cm^{-1}]
Weld Q8	1	264.1	25.5	0.500	8.08
	2	264.4	25.5	0.496	8.16
Weld Q9	1	324.1	27.7	0.590	9.13
	2	321.3	27.8	0.599	8.95
Weld Q10	1	267.3	25.5	0.401	10.22
	2	265.1	25.6	0.406	10.03
Weld Q12	1	252.5	23.1	0.296	11.82
	2	250.5	23.2	0.296	11.78
Weld Q14	1	267.4	25.5	0.291	14.06
	2	267.7	25.6	0.293	14.03

Welds could dilate freely in the jig, which caused deformation of both web and flange. Because the welded samples were loaded only in the flange direction, the angular deformation after the 1st and 2nd weld bead was measured in accordance with schematic Figure 4. Totally, deformation was measured at 11 points in the direction of weld length, á 30 mm (distance between individual points). Table 5 shows the average values of angular deformation after welding the 1st and 2nd weld bead.

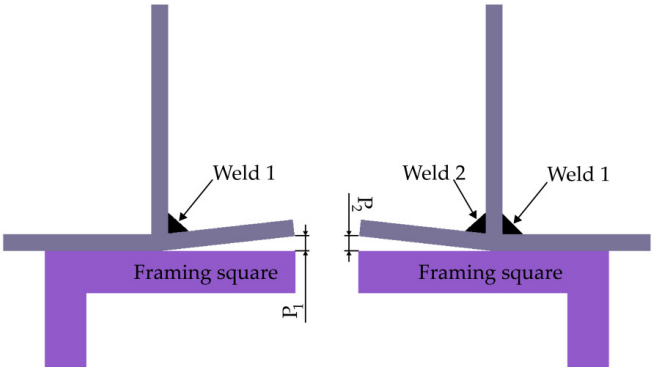

Figure 4. Measurement of the angular deformation after welding.

Table 5. Magnitudes of the angular deformation for relevant welds.

Bead/Weld	Weld Q8	Weld Q9	Weld Q10	Weld Q12	Weld Q14
Bead 1 (P_1)	1.23 ± 0.17	1.43 ± 0.13	1.39 ± 0.11	1.41 ± 0.14	1.37 ± 0.14
Bead 2 (P_2)	2.71 ± 0.15	3.21 ± 0.24	3.16 ± 0.18	3.18 ± 0.17	3.34 ± 0.26

4. Preparation of Fatigue Testing Samples and Geometrical Evaluation of Welds

For all welded joints, the initial 35 mm and final 35 mm of weld length were removed so that the samples supposed to determine fatigue life were taken from the steady temperature field. From this area, testing samples for fatigue life tests were cut out with a width of 18 mm, as it is schematically shown in Figure 5a. Because there was effort to load the samples in the flange direction for our own cyclic loading experiments, the web was removed at a sufficient distance from the weld. To avoid the notch effect after cutting the testing material, edges of each sample were machined by surface grinding under intense cooling to avoid negative thermal influence. An example of the actual completely prepared testing sample is subsequently shown in Figure 5b. Modal analysis using software Autodesk Fusion 360 (version 2.0.9006, Autodesk, Mill Valley, USA) was performed for the designed shape and clamping method. It was found that natural frequency of the sample was 17.4 kHz, which was significantly higher than the finally applied loading frequency (20 Hz).

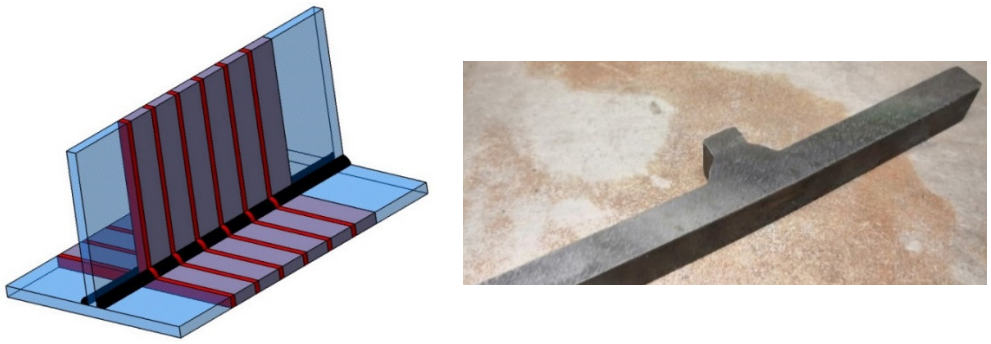

(**a**) (**b**)

Figure 5. Cyclic testing: (**a**) cutting of testing samples; (**b**) completely prepared testing sample.

Moreover, a geometrical evaluation of both weld beads was performed as it is schematically shown in Figure 6 for all welds. There was measured the actual throat thickness of the fillet weld **a**, weld width **w**, and the maximal penetration depth **x**. Possible weld asymmetry is expressed by dimensions $\mathbf{Z_1}$ and $\mathbf{Z_2}$. In addition to that, there was also measured the width of the heat-affected zone (HAZ) in the flange direction that is marked as **HAZf**, and in the web direction marked as **HAZw**. The last measured quantity was the radius between the base material and weld on the flange side marked as **R**.

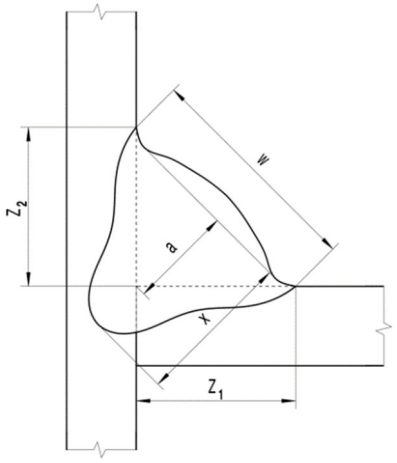

Figure 6. Schematic illustration of the geometrically evaluated quantities of weld.

In Table 6 are summarized the geometrical quantities for all weld beads and heat input values. Subsequently, in the following figures (Figures 7–11) are graphically shown the metallographic samples of all welds, including geometrical evaluation in accordance with Figure 6.

Table 6. Geometrical evaluation of the monitored weld beads.

Weld Designation	Number of Bead	Measured Parameter [mm]							
		a	x	w	Z_1	Z_2	HAZf	HAZw	R
Weld Q8	1	3.80	5.04	7.60	5.50	5.25	1.36	1.22	1.27
	2	3.86	5.40	7.77	5.74	5.23	1.34	1.34	1.28
Weld Q9	1	4.07	7.20	8.13	5.59	5.91	1.48	1.37	1.25
	2	4.02	7.38	8.05	5.85	5.52	1.43	1.03	1.21
Weld Q10	1	4.11	5.41	8.24	6.10	5.54	1.54	1.44	1.45
	2	4.27	5.87	8.56	6.31	5.80	1.41	1.34	1.49
Weld Q12	1	4.73	5.81	9.48	6.95	6.46	1.87	1.61	0.98
	2	4.51	5.28	9.13	7.01	5.86	1.65	1.56	1.02
Weld Q14	1	5.12	6.88	10.21	7.28	7.17	1.81	1.84	0.94
	2	5.17	6.82	10.34	7.49	7.15	1.94	1.78	1.07

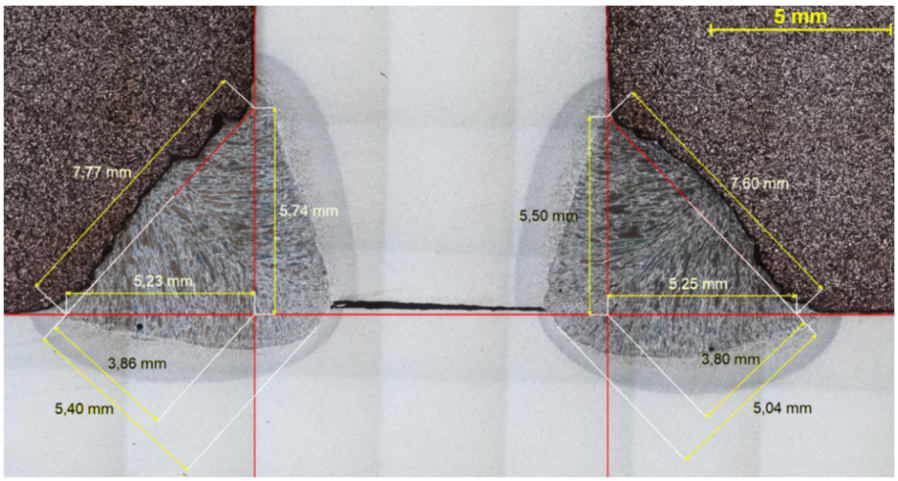

Figure 7. Metallographic sample of Weld Q8 (Q = 8 kJ·cm^{-1})—1st bead (right) and 2nd bead (left).

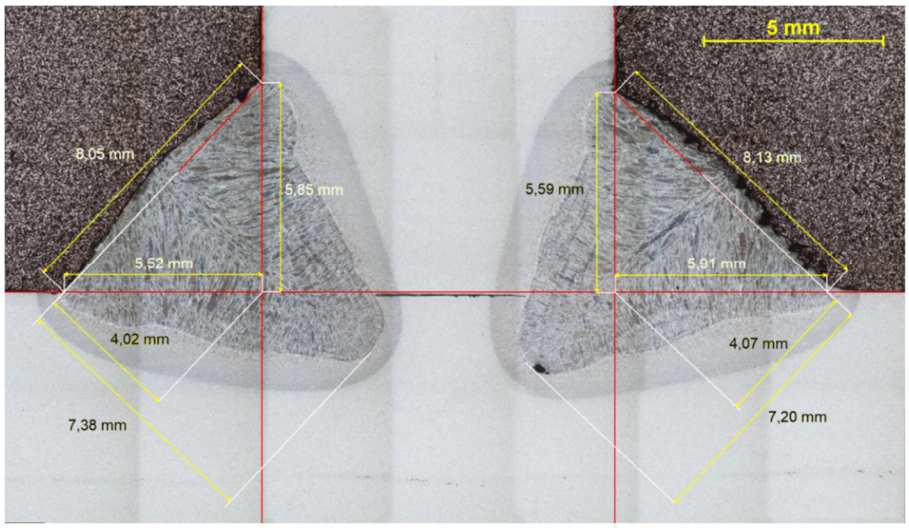

Figure 8. Metallographic sample of Weld Q9 (Q = 9 kJ·cm^{-1})—1st bead (right) and 2nd bead (left).

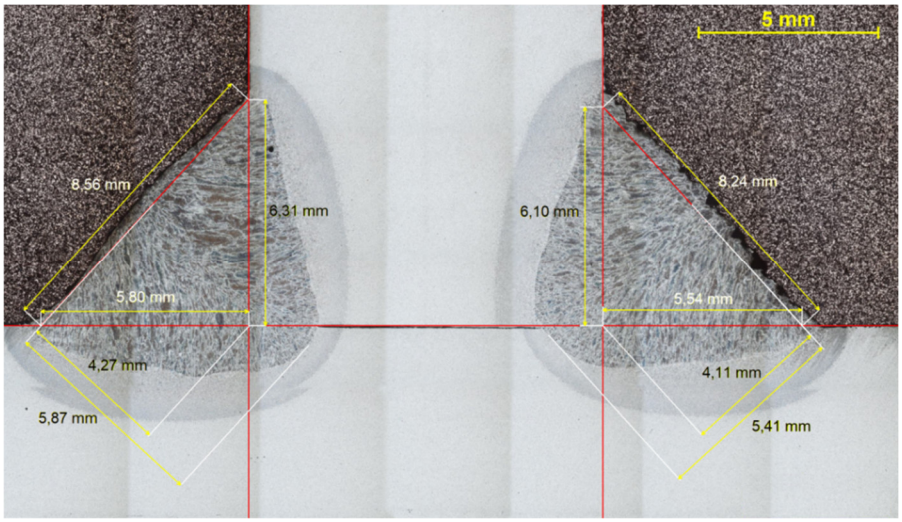

Figure 9. Metallographic sample of Weld Q10 (Q = 10 kJ·cm^{-1})—1st bead (right) and 2nd bead (left).

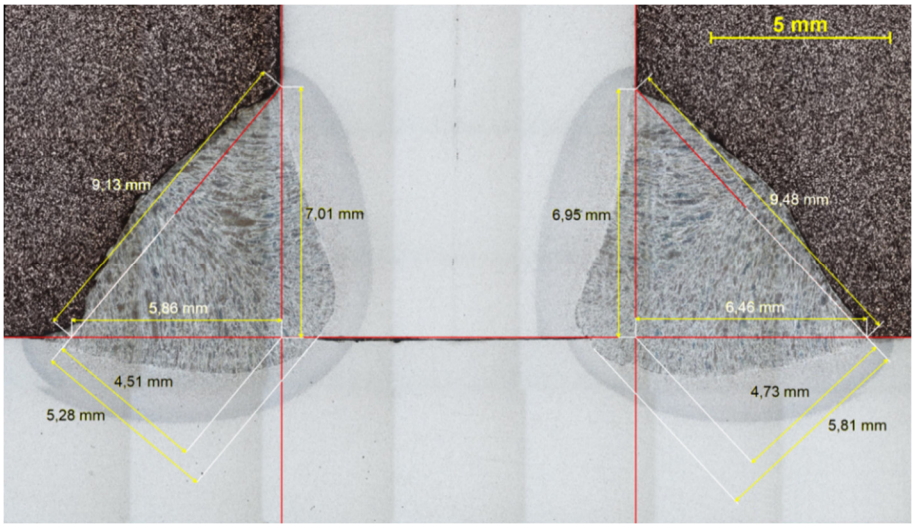

Figure 10. Metallographic sample of Weld Q12 (Q = 12 kJ·cm^{-1})—1st bead (right) and 2nd bead (left).

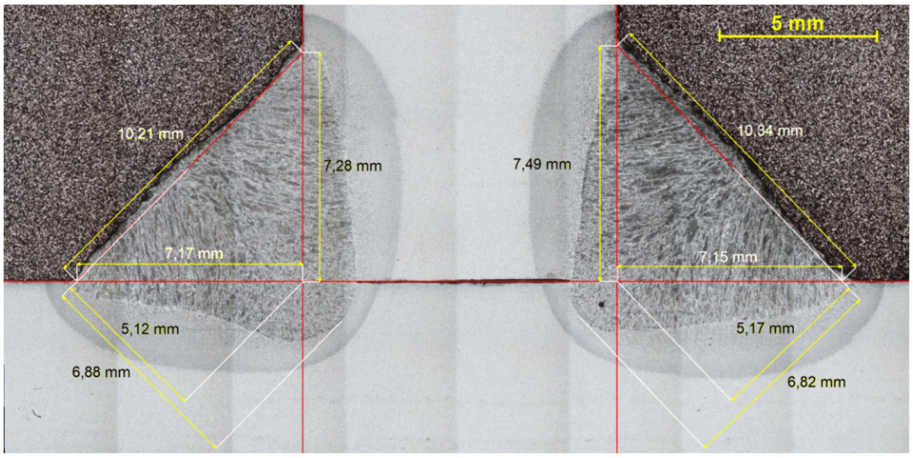

Figure 11. Metallographic sample of Weld Q14 (Q = 14 kJ·cm^{-1})—1st bead (right) and 2nd bead (left).

5. Fatigue Life Determination for Tested Fillet Welds

As in the case of the base material, a servo-hydraulic testing machine INOVA FU-O-1600-V2 (INOVA GmbH, Bad Schwalbach, Germany) in the controlled force mode was used to determine the fatigue life of welded joints. Based upon the results of the initial fatigue tests (for base material), the

samples were loaded under the following stress amplitudes: 300, 240, 170, 152.5, 135, 117.5, 100, 82.5, 74 and 65 MPa. Furthermore, in this case, all samples were subjected to a fully reversed harmonic cycle (purely alternating stress) with stress ratio R = −1. Compared to the fatigue testing of the base material, the loading frequency was lower by 20 Hz due to the larger cross-section area of testing samples—thus also higher force amplitudes. This causes an increase of the strain rate in the sample, which led to a heating of the sample surface under a frequency of 40 Hz. As in the case of the base material, there were firstly carried out primary tests of samples with double-sided fillet welds and having corresponding dimensions and a preparation method that was subsequently used for our own experiment. The grinded surface of the sample was again scanned by an infrared pyrometer on the interface between the weld bead and base material. Such primary testing was performed at stress amplitudes 300 and 175 MPa. The same test termination criteria were also used in this kind of fatigue test—fatigue crack initialization or achieving the fatigue limit at 10^7 cycles, where testing material does not show a distinct fatigue limit σ_C.

Identification of the crack initiation was realized on the basis of setting the testing machine INOVA FU-O-1600V2 control program. The criterion of the so-called unstable increase of deformation during the test was chosen to terminate our own testing procedure. This criterion is based on the continuous monitoring of the sample deformation (to be specific, its deviation) necessary to achieve the required loading force. Such monitored strain magnitude is averaged from the last 500 test cycles and thus allows the elimination of the strengthening or recovery effect of the sample without termination of the test. The testing procedure was terminated when deformation revealed an abnormal increase of more than 20% compared to the average of the last 500 cycles. After termination of every test, there was loaded a course force vs. displacement by return, from which it was possible to identify the moment of crack initialization. In all cases presented in this paper, crack in the joint was identified after test termination.

All welds were loaded in the flange direction, as it is schematically shown in Figure 12. Subsequently, Table 7 then gives an overview about fatigue test results for all tested welds.

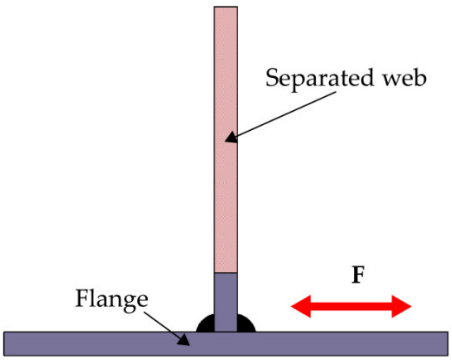

Figure 12. Shape adjustment and loading mode of fatigue tests.

Table 7. Cycles to failure N_f in dependence on stress amplitudes σ_A for the monitored welds.

Stress Amplitude	Cycles to Failure N_f [1]				
σ_A [MPa]	Weld Q8	Weld Q9	Weld Q10	Weld Q12	Weld Q14
300	10,436	10,398	10,513	10,279	10,187
240	31,093	30,268	31,825	29,245	28,451
170	74,840	67,417	86,153	55,668	59,627
152.5	111,389	103,284	135,381	95,676	102,477
135	167,536	132,982	201,117	190,961	163,448
117.5	242,359	236,172	346,740	173,615	173,397
100	1,057,662	515,809	546,096	359,291	253,974
82.5	1,147,041	813,423	793,318	701,936	660,143
74	6,356,012	3,983,642	3,011,738	2,451,977	2,282,815
65	$>10^7$	$>10^7$	$>10^7$	$>10^7$	$>10^7$

In all cases, the location of the fatigue failure of the testing sample was determined, and the crack was initiated at the interface between the flange and the weld bead, as it is obvious from Figure 13a for Weld Q12 (stress amplitude σ_A = 300 MPa) and in Figure 13b for Weld Q12 (stress amplitude σ_A = 74 MPa). In all fatigue failures, the crack grew perpendicularly to the loading force direction. In addition to that, a fatigue limit σ_C = 65 MPa was determined for all fillet welds, which represents only 20% of the fatigue (endurance) limit σ_C measured for the unaffected base material.

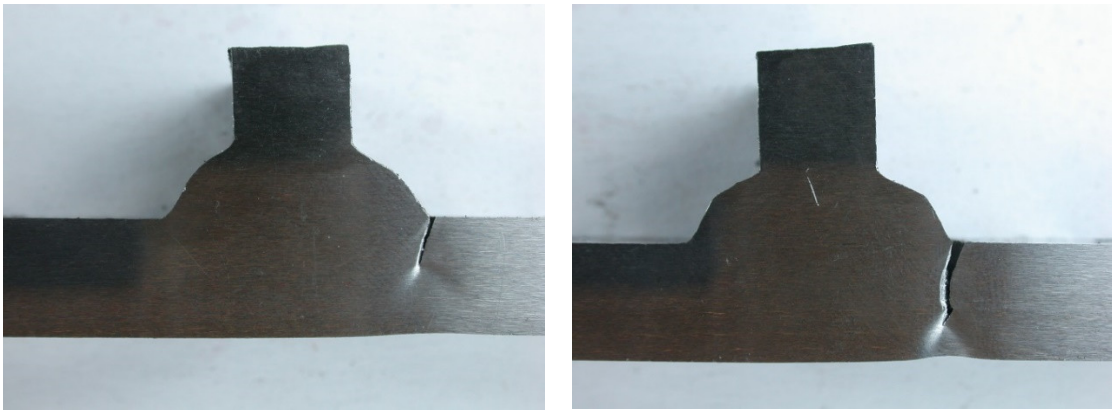

(**a**) (**b**)

Figure 13. Location of crack initialization for Weld Q12: (**a**) σ_A = 300 MPa; (**b**) σ_A = 74 MPa.

Results summarized in Table 7 were subsequently plotted in the S-N curves (log-log scale) to determine fatigue characteristics via their approximation according to the so-called Basquin's equation (Equation (1)):

$$\sigma_A = \sigma_f \cdot (2N_f)^b \quad (1)$$

In Equation (1), σ_f (MPa) is the fatigue strength coefficient and b (1) is the fatigue strength exponent. By these approximation quantities can be characterized the whole course of the fatigue life (via stress amplitude σ_A as the independent variable) vs. cycles to failure N_f (independent variable). However, in this case are instead of cycles to failure N_f are used so-called reversals to failure—thus $2N_f$.

Generally, Basquin's equation mathematically means the power-law function. Because of better clearness (specially to cover large values of reversals to failure), in graphs this equation is shown in log-log scales, thus as the linear function. In Table 8 are summarized results of fatigue strength coefficient σ_f and fatigue strength exponent b for monitored heat input values.

Table 8. Values of fatigue strength coefficient σ_f and fatigue strength exponent b (computed according to Basquin's equation) for the monitored fillet welds.

Weld Designation	Average Heat Input Q [kJ·cm^{-1}]	Fatigue Strength Coefficient σ_f [MPa]	Fatigue Strength Exponent b [1]
Weld Q8	8.12	2715 ± 293	−0.230 ± 0.020
Weld Q9	9.04	3534 ± 359	−0.255 ± 0.021
Weld Q10	10.13	4427 ± 304	−0.270 ± 0.015
Weld Q12	11.80	4438 ± 419	−0.276 ± 0.021
Weld Q14	14.05	4704 ± 481	−0.281 ± 0.023

6. Discussion

The welding heat input strongly affects the basic mechanical properties (e.g., such as yield strength, ultimate tensile strength, and ductility) of fine-grained steels [4,6,20,21]. Higher heat input values cause a longer exposition to high temperatures, which means more intense changes that can

occur in HAZ of welds. In addition to that, these changes influence not only the mechanical properties, but also have a very significant effect on the notch toughness value [4,6,22].

In addition to the changes that occur in the HAZ, other aspects also have an effect on the reduction of fatigue life in the case of cyclic loading. Especially important is the effect of the weld bead geometry, because it defines the notch effect at cyclic loading as well as, e.g., the magnitude of angular deformations after welding, causing occurrence of the combined stress (tension, compression, and bending). To define the influence of the individual aspects mentioned above is very difficult under dynamic loading, especially in the case of fillet welds. To keep the boundary conditions as accurate as possible, all samples used for fatigue tests had exactly the same dimensions, grinded edges with the same surface roughness, and completely identical loading conditions (clamping force, frequency, sample centering in jaws, and so on). Regarding the actual knowledge in the field of welding fine-grained thermomechanically processed structural steels, there would be expected a reduction of the welded joint fatigue life with increasing heat input value. This assumption is also confirmed in this research by the slope of linear fitting, as shown in Figure 14, expressed via values σ_f and b computed from Basquin's equation (linear fitting of measured data from Table 7). The lowest slope (b = −0.230) was computed for tested welded joints with the heat input of Q = 8 kJ·cm^{-1}. Generally stated, the higher the heat input value, the higher the slope of the obtained trends. These results are usually used by designers when designing the maximal allowable loads of different steel welded structures.

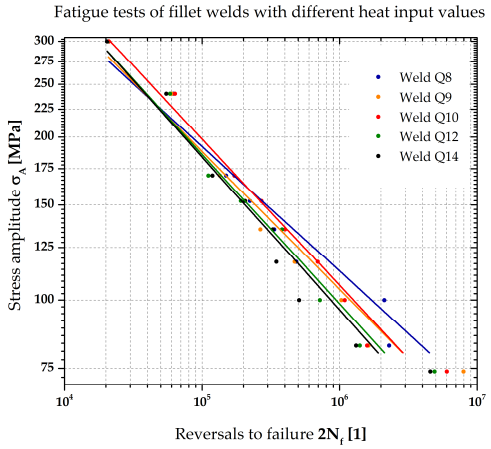

Figure 14. S-N curves (log-log scale)—graphical comparison of the measured trends (linear fitting according to Basquin's equation) for fillet welds with different heat input values.

However, from Figure 14 is also evident that different slopes of fitted linear trends no longer fully confirm the assumption about reduction in the fatigue life with increasing heat input value in the whole range of applied stress amplitudes. In the area of limited life, and especially in its initial phase at higher stress amplitudes σ_A (up to 225 MPa), better results were achieved with higher heat input values—thus for Q10, Q12, and Q14. This would correspond to weldments with an expected number of cycles not exceeding 45,000 cycles. On the other hand, from this value slopes of applied linear trends behave according to the theoretical assumptions. A partial exception can be observed only in the case of the trend determined for Weld Q10, where are achieved the lower values of fatigue life—lower than 162 MPa compared to Weld Q8 and lower even than 83 MPa compared to Weld Q9. This partial anomaly is probably caused by the given weld geometry, as shown in Table 6, where the highest value of radius R was measured for Weld Q10 at the interface between the weld and flange. Thus, there is partially reduced the notch effect as a stress concentrator under cyclic loading.

However, taking into account the error measurement of the fatigue strength coefficient and especially the fatigue strength exponent, as shown in Table 8, which vary from 6% to 9% for the individual heat input values, it can be stated that heat input value does not influence the change of fatigue limit in the low cycle fatigue area. On the other hand, influence of the heat input can be observed in the high cycle fatigue area, where the difference of fatigue limit $\sigma_{c(W)}$ for curves with the

heat input value Q = 8 kJ·cm^{-1} and Q = 14 kJ·cm^{-1} is about 30%, even when the maximal overlap confidence intervals are taken into account. Based on the above findings, it could be expected that heat input value will also affect the magnitude of the fatigue limit $\sigma_{c(W)}$. Nevertheless, as it is shown in Table 7, this magnitude of $\sigma_{c(W)}$ for cycles to failure $N_f > 10^7$ was the same (65 MPa) for all tested heat input values. Based upon the cycles to failure measured at stress amplitude σ_A = 74 MPa, it can be assumed that for welded joints having lower heat input values, the fatigue limit would be reached even at stress amplitudes higher than 65 MPa.

Comparing the obtained results with other similar works, it can be stated that different research works in the field of HSLA steels' fatigue life are carried out by many researchers, but not for fillet welds. Šebestová et al. [10], determining the fatigue life of welds for S460MC and S700MC steels, performed by the Laser-hybrid method, measured for base material steel 460MC a fatigue limit of σ_c = 310 MPa and fatigue limits of butt welds (in dependence on the heat input value) of about 100 MPa. The fatigue limit of base material was lower by 30 MPa than fatigue limit σ_c measured here. The reason for that was most likely the square cross-section area of the testing samples, where fatigue cracks can more easily initiate in the corners of the sample. The fatigue (endurance) limit of butt welds is usually 2 to 3 times higher than that of fillet welds. Lahtinen et al. [12] tested fatigue properties of butt welds made of S700MC steel and welded by the MAG method. The effect of the input heat was there expressed by a different time value $t_{8/5}$. As in our case, it was confirmed that the effect of the heat input value (expressed by the slope of fitting linear trends arising from the measured values) has a much higher influence just at lower stress amplitudes corresponding to the cycles to failure of about 180,000 cycles.

Another important finding is also the mutual ratio between the yield strength of tested material R_e, fatigue limit of the base material $\sigma_{c(BM)}$, and fatigue limit of the welded joint $\sigma_{c(W)}$. These ratios are for the tested material S460MC as follows: $\sigma_{c(BM)}/R_e$ = 0.625; $\sigma_{c(W)}/R_e$ = 0.119; and $\sigma_{c(W)}/\sigma_{c(BM)}$ = 0.193. For steel S700MC they are: $\sigma_{c(BM)}/R_e$ = 0.583 [14]; $\sigma_{c(W)}/R_e$ = 0.102 [17]; and $\sigma_{c(W)}/\sigma_{c(BM)}$ = 0.171. From these ratios it is evident that applications of materials with higher yield strength does not automatically mean achieving relatively higher values of welded joint fatigue life. Therefore, it is very important to consider other aspects, such as the structural design of joints, welding parameters influencing weld geometry (notch effect), as well as our own welding method causing angular deformation.

7. Conclusions

Fine-grained HSLA steels, and especially steels with yield strength lower than 550 MPa, are nowadays founding a wide range of their applications—mainly in the automotive industry. The major reason for that rests in constant deformation behavior of these materials during cold forming. Stability of the properties is given by the chemical composition of these steels, monitored mainly due to the carbon content and used micro-alloys. Both thermomechanically processed steels with a higher yield strength and thermomechanically processed steels with a lower yield strength require specific welding procedures, and in particular, with regard to reduction of the heat input value. Major experimentally obtained knowledge about solved issues can be summarized in the following points:

1. Circular and rectangular cross-sections areas of testing samples in accordance with standard EN 3987 can be used to determine the fatigue properties of the base material. However, it should be taken into account that due to the shape of their cross-section areas, magnitudes of the fatigue limit $\sigma_{C(BM)}$ can varied by up to 10%.
2. Welded joints significantly reduce fatigue properties both in the area of limited fatigue life and infinite life—fatigue limit $\sigma_{C(W)}$. In the case of steel S460MC and a double-sided fillet weld, the fatigue limit was reduced by 80%. Interestingly, this reduction is even higher in the case of welds from materials with higher yield strengths and values of the fatigue limit $\sigma_{C(W)}$ are approaching each other.
3. The biggest influence on such a significant reduction of σ_C is mainly given by the notch effect of the fillet weld. Influence of the heat input value on the fatigue limit σ_c was not determined, because in all cases was achieved $\sigma_{C(W)}$ = 65 MPa. The reason may be too rough a step at applied stress amplitudes (74 and 65 MPa).

4. However, the heat input value was reflected in the area of limited fatigue life. Nevertheless, this effect is not uniform over all monitored stress amplitudes. At higher stress amplitudes, such an effect is very small. If the measurement errors are taken into account, there can be stated that the heat input influence does not take effect in the low cycle fatigue test. At low stress amplitudes (σ_A = 82.5 and 74 MPa), the effect is already significant and differences between welds with the heat input value Q = 8 kJ·cm^{-1} and Q = 14 kJ·cm^{-1} are 42% and 64% (again in light of cycles to failure), respectively. In the case of comparing the values of approximation constants, as shown in Table 8, from fitting trends, these differences are as follows—41% and 44%, respectively. When the maximal overlap of the confidence intervals is taken into account, the difference will be almost 30%.
5. During cyclic loading, the fatigue life is certainly also influenced by additional bending stress caused by the angular deformation of the testing samples. However, it is very problematic to quantify the effect of such additional bending stress and its assessment will be the subject of further works. Nevertheless, based on the obtained results, it can be stated that the difference in the additional bending moment during cyclic loading of Welds Q9, Q10, and Q12 (so with higher heat input values) was lower than 1%. For Weld Q14 it was lower than 5%. Smaller angular deformation was achieved only for Weld Q8—namely by 15%.

The achieved results can be interpreted as the following:

1. In the area of low cycle fatigue, the influence of the heat input is negligible. Therefore, more attention should be paid to the arc welding process parameters, which define the weld geometry and thus the notch effect as well.
2. On the other hand, the influence of the heat input value already took place in the area of high cycle fatigue. That is why this fact should be taken into account when designing the dynamically loaded structural components with a planned service life up to 2·× 10^6 cycles. We recommend considering the fatigue limit $\sigma_{c(W)}$ of the fillet welded joint when designing structures with the planned number of cycles over 2·× 10^6. In this case, the effect of heat input may not be taken into account.
3. It is also a suitable and beneficial finding that the mutual ratio $\sigma_{c(W)}/\sigma_{c(BM)}$ and $\sigma_{c(W)}/R_e$ is decreasing with the increasing magnitude of yield strength. This fact should be also taken into account during engineering computations and design. The standard approach is to choose materials with higher strength to improve fatigue life. However, it is not very effective in light of a decreasing ratio $\sigma_{c(W)}/R_e$ and can hardly compensate for increased material costs and worse weldability. This is, of course, valid under the presumption that the notch effect is not reduced by grinding of the weld.

Author Contributions: Conceptualization, J.M. and P.S.; Methodology and Resources, J.M. and R.T.; Investigation, J.M., J.S., P.S. and R.T.; Data curation, Writing—Review and Editing and Visualization, J.M. and J.S.; Writing—original draft preparation, J.M. All authors have read and agreed to the published version of the manuscript.

Funding: This work was supported by the Student Grant Competition of the Technical University of Liberec under the project No. SGS-2020-5008.

Conflicts of Interest: The authors declare no conflict of interest.

References

1. Barbaro, F.; Kuzmikova, L.; Zhu, Z.; Li, H. Weld Haz Properties in Modern High Strength Niobium Pipeline Steels. In *Energy Materials 2014*; Springer International Publishing: Cham, Switzerland, 2016; pp. 657–664.
2. Fernández, J.; Illescas, S.; Guilemany, J.M. Effect of microalloying elements on the austenitic grain growth in a low carbon HSLA steel. *Mater. Lett.* **2007**, *61*, 2389–2392, doi:10.1016/j.matlet.2006.09.021.
3. Illescas, S.; Fernández, J.; Asensio, J.; Sánchez-Soto, M.; Guilemany, J.M. Study of the mechanical properties of low carbon content HSLA steels. *Rev. Metal.* **2009**, *45*, 424–431, doi:10.3989/revmetalm.0902.

4. Moravec, J.; Novakova, I.; Sobotka, J.; Neumann, H. Determination of Grain Growth Kinetics and Assessment of Welding Effect on Properties of S700MC Steel in the HAZ of Welded Joints. *Metals* **2019**, *9*, 707, doi:10.3390/met9060707.
5. Wang, F.; Strangwood, M.; Davis, C. Grain growth during reheating of HSLA steels with a narrow segregation separation. *Mater. Sci. Technol.* **2019**, *35*, 1963–1976, doi:10.1080/02670836.2019.1658440.
6. Mičian, M.; Harmaniak, D.; Nový, F.; Winczek, J.; Moravec, J.; Trško, L. Effect of the $t_{8/5}$ Cooling Time on the Properties of S960MC Steel in the HAZ of Welded Joints Evaluated by Thermal Physical Simulation. *Metals* **2020**, *10*, 229, doi:10.3390/met10020229.
7. Branco, R.; Berto, F. Mechanical Behavior of High-Strength, Low-Alloy Steels. *Metals* **2018**, *8*, 610, doi:10.3390/met8080610.
8. Jambor, M.; Ulewicz, R.; Nový, F.; Bokůvka, O.; Trško, L.; Mičian, M.; Harmaniak, D. Evolution of microstructure in the heat affected zone of S960MC GMAW weld. *Mater. Res. Proc.* **2018**, *5*, 78–83.
9. Njock Bayock, F.; Kah, P.; Mvola, B.; Layus, P. Effect of Heat Input and Undermatched Filler Wire on the Microstructure and Mechanical Properties of Dissimilar S700MC/S960QC High-Strength Steels. *Metals* **2019**, *9*, 883, doi:10.3390/met9080883.
10. Šebestová, H.; Horník, P.; Mrňa, L.; Jambor, M.; Horník, V.; Pokorný, P.; Hutař, P.; Ambrož, O.; Doležal, P. Fatigue properties of laser and hybrid laser-TIG welds of thermo-mechanically rolled steels. *Mater. Sci. Eng. A* **2020**, *772*, 138780, doi:10.1016/j.msea.2019.138780.
11. Keeler, S.; Kimchi, M. *Advanced High-Strength Steels Application Guidelines V5*; WorldAutoSteel: Brussels, Belgium, 2015.
12. Lahtinen, T.; Vilaça, P.; Infante, V. Fatigue behavior of MAG welds of thermo-mechanically processed 700MC ultra high strength steel. *Int. J. Fatigue* **2019**, *126*, 62–71, doi:10.1016/j.ijfatigue.2019.04.034.
13. Corigliano, P.; Crupi, V.; Epasto, G.; Guglielmino, E.; Risitano, G. Fatigue life prediction of high strength steel welded joints by Energy Approach. *Procedia Struct. Integr.* **2016**, *2*, 2156–2163, doi:10.1016/j.prostr.2016.06.270.
14. Lago, J.; Trško, L.; Jambor, M.; Nový, F.; Bokůvka, O.; Mičian, M.; Pastorek, F. Fatigue Life Improvement of the High Strength Steel Welded Joints by Ultrasonic Impact Peening. *Metals* **2019**, *9*, 619, doi:10.3390/met9060619.
15. Kim, Y.; Hwang, W. Effect of weld seam orientation and welding process on fatigue fracture behaviors of HSLA steel weld joints. *Int. J. Fatigue* **2020**, *137*, 105644, doi:10.1016/j.ijfatigue.2020.105644.
16. Bandgar, S.; Gupta, C.; Rao, G.; Malik, P.; Singh, R.N.; Sridhar, K. Fatigue Crack Growth Rate Behaviour of HSLA Steel at Varying Load Amplitudes. *Procedia Struct. Integr.* **2019**, *14*, 330–336, doi:10.1016/j.prostr.2019.05.041.
17. Krasnowski, K. Influence of High Frequency Impact Treatment (HiFIT) on fatigue strength of welded joints of high-strength steel S700MC for bridges applications. *IOP Conf. Ser. Mater. Sci. Eng.* **2018**, *419*, 012020, doi:10.1088/1757-899X/419/1/012020.
18. Holmstrand, T.; Mrdjanov, N.; Barsoum, Z.; Åstrand, E. Fatigue life assessment of improved joints welded with alternative welding techniques. *Eng. Fail. Anal.* **2014**, *42*, 10–21, doi:10.1016/j.engfailanal.2014.03.012.
19. Skriko, T.; Ghafouri, M.; Björk, T. Fatigue strength of TIG-dressed ultra-high-strength steel fillet weld joints at high stress ratio. *Int. J. Fatigue* **2017**, *94*, 110–120, doi:10.1016/j.ijfatigue.2016.09.018.
20. Górka, J. Microstructure and properties of the high-temperature (HAZ) of thermo-mechanically treated S700MC high-yield-strength steel. *Mater. Tehnol.* **2016**, *50*, 616–621, doi:10.17222/mit.2015.123.
21. Górka, J. Influence of the maximum temperature of the thermal cycle on the properties and structure of the HAZ of steel S700MC. *IOSR J. Eng.* **2013**, *3*, 22–28, doi:10.9790/3021-031142228.
22. Schmidová, E.; Bozkurt, F.; Culek, B.; Kumar, S.; Kuchariková, L.; Uhríčik, M. Influence of Welding on Dynamic Fracture Toughness of Strenx 700MC Steel. *Metals* **2019**, *9*, 494, doi:10.3390/met9050494.